

https://dspace.org/

Invariance of Mitochondria and Synapses in the Primary Visual Cortex of Mammals Provides Insight Into Energetics and Function

M T Karl; Y D Kim; K Rajendran; Paul Manger; C C Sherwood

WILEY-BLACKWELL
https://hdl.handle.net/10539/42488
WOS

Downloaded from a DSpace repository. https://dspace.org/

Check for updates

Journal of Comparative Neurology

WILEY

JCN RESEARCH IN SYSTEMS NEUROSCIENCE THE JOURNAL OF COMPARATIVE NEUROLOGY

RESEARCH ARTICLE

Invariance of Mitochondria and Synapses in the Primary Visual Cortex of Mammals Provides Insight Into Energetics and Function

Molly T. Karl[1,2] | Young Do Kim[1] | Kavita Rajendran[1] | Paul R. Manger[3] | Chet C. Sherwood[1]

[1]Department of Anthropology and Center for the Advanced Study of Human Paleobiology, The George Washington University, Washington, District of Columbia, USA | [2]Department of Anatomy and Cell Biology, School of Medicine and Health Sciences, The George Washington University, Washington, District of Columbia, USA | [3]Faculty of Health Sciences, School of Anatomical Sciences, University of the Witwatersrand, Johannesburg, South Africa

Correspondence: Chet C. Sherwood (sherwood@gwu.edu)

Received: 10 February 2024 | **Revised:** 16 August 2024 | **Accepted:** 30 August 2024

Funding: This research was supported by National Science Foundation (Grants EF-2021785 and DRL-2219759) and National Institutes of Health (Grants HG011641 and NS092988).

Keywords: brain evolution | energy | mammals | mitochondria | neocortex | RRID:SCR_008515 | RRID:SCR_021162 | synapse

ABSTRACT

The cerebral cortex accounts for substantial energy expenditure, primarily driven by the metabolic demands of synaptic signaling. Mitochondria, the organelles responsible for generating cellular energy, play a crucial role in this process. We investigated ultrastructural characteristics of the primary visual cortex in 18 phylogenetically diverse mammals, spanning a broad range of brain sizes from mouse to elephant. Our findings reveal remarkable uniformity in synapse density, postsynaptic density (PSD) length, and mitochondria density, indicating functional and metabolic constraints that maintain these fundamental features. Notably, we observed an average of 1.9 mitochondria per synapse across mammalian species. When considered together with the trend of decreasing neuron density with larger brain size, we find that brain enlargement in mammals is characterized by increasing proportions of synapses and mitochondria per cortical neuron. These results shed light on the adaptive mechanisms and metabolic dynamics that govern cortical ultrastructure across mammals.

1 | Introduction

Mammalian brains exhibit diversity in size and anatomy (Assaf et al. 2020; Barton and Harvey 2000; Boddy et al. 2012; Smaers et al. 2021), which is associated with differences in cognitive abilities and sensorimotor processing capacities (DeCasien and Higham 2019; Englund and Krubitzer 2020; Fox, Muthukrishna, and Shultz. 2017; Heldstab et al. 2016; MacLean et al. 2014). The cerebral cortex displays especially remarkable phylogenetic variation in neural tissue composition and function (DeFelipe, Alonso-Nanclares, and Arellano 2002; Falcone et al. 2019; La Rosa et al. 2020; Nguyen et al. 2020; Sherwood et al. 2009). Although research has focused on the scaling of cellular distributions and neuron morphology in the neocortex (Beaulieu-Laroche et al. 2021; Elston et al. 2011; García-Cabezas and Zikopoulos 2019; Galakhova et al. 2022; Haug 1987; Herculano-Houzel 2009; Herculano-Houzel, Manger, and Kaas 2014; Stimpson et al. 2023; Tower 1954), less is known about the comparative ultrastructure of this brain region across mammals.

Studies of the neocortex at the ultrastructural level can offer valuable insights into intracellular organelles, such as mitochondria (Chan 2006; Else and Hulbert 1985; Friedman and Nunnari 2014; Hara et al. 2014; Kukat et al. 2011; Morozov et al. 2017;

© 2024 Wiley Periodicals LLC.

Yu et al. 2020), and intercellular structures, like synapses (Alonso-Nanclares et al. 2008, 2023; DeFelipe et al. 1999; Sherwood et al. 2020), which participate in cell-to-cell communication. Cellular communication is an energetically demanding process (Attwell and Laughlin 2001; Harris, Jolivet, and Attwell 2012; Hyder, Rothman, and Bennett 2013; Lennie 2003; Magistretti and Allaman 2015), and understanding the underlying metabolic machinery is crucial. However, the relationship between energetic requirements and brain tissue composition across mammalian species remains uncertain (Herculano-Houzel 2011; Hyder, Rothman, and Bennett 2013; Magistretti and Allaman 2015; Sokoloff 1981; Vannucci et al. 1998; Ventura-Antunes, Dasgupta, and Herculano-Houzel 2022). Thus, it may be informative to examine metabolic and connectional architecture, such as mitochondria and synapses, in a comparative study encompassing diverse mammalian brains that vary in size.

Despite several studies exploring synapse density across different mammalian species (Alonso-Nanclares et al. 2023; Colonnier and Beaulieu 1985; DeFelipe et al. 1999; Sherwood et al. 2020), comparative data on mitochondria numbers in the neocortex remain limited. Synapses rely heavily on mitochondria, evident from their abundance and proximity to synaptic clefts (Hara et al. 2014; Hollenbeck 2005; Ly and Verstreken 2006; Picard 2015). Research on the relationship between mitochondria and synapses can offer crucial insights into brain metabolism and its implications for neural function.

In this study, we investigated the scaling relationships of ultrastructure in the primary visual cortex (Area V1) across a diverse sample of 18 mammalian species (2 marsupial species and 16 eutherian species) focusing on four key variables: synapse density, postsynaptic density (PSD) length, mitochondria density, and neuron density. The PSD is a complex network of proteins that cluster around the neurotransmitter receptors at the synapse and functions in signaling and plasticity (Liu et al. 2019). By systematically examining these ultrastructural features across a broad range of brain sizes and phylogenetic backgrounds, our objective was to determine whether there is an allometric scaling relationship, or if these variables remain relatively constant due to their fundamental functional roles.

The well-established homology and relatively conserved function of cortical Area V1 across mammals were the basis for selecting this region of interest (Krubitzer 1995; Kaas 2013). Area V1 is associated with early visual processing, receiving direct input from the lateral geniculate nucleus of the thalamus, and forming an early stage in the visual pathway of the neocortex (Douglas and Martin 2004). The sample of species used in this study was chosen to encompass a broad spectrum of brain size variation across phylogenetically diverse mammals. This included representatives from macropodid marsupials, afrotherians, xenarthrans, artiodactyls, carnivores, rodents, and primates. The largest brain in the sample was from an African bush elephant (*Loxodonta africana*) which is more than 12,000 times larger than the smallest brain in the sample from a mouse (*Mus musculus*). Within the primate group, we included representatives from strepsirrhines, platyrrhines, cercopithecids, and hominoids (including humans).

An additional aim of this research was to examine whether ultrastructural features of cortical Area V1 differ in primates compared to other mammals. Primates have exceptional visual abilities, which are underpinned by specializations of the nervous system (Kaas 2012; Leopold, Mitchell, and Freiwald 2017). Binocular and stereoscopic visions are key adaptations shared by all primates, which enable precise depth perception and object localization. Moreover, haplorrhine primates exhibit especially high visual acuity, aided by the presence of a fovea, a small central region in the retina with an enhanced density of photoreceptors. Some primate species also have trichromatic vision, which is facilitated by the possession of three different types of cone photoreceptors that provide color discrimination capabilities (Heesy and Ross 2001). Within Area V1, a distinctive feature of primates is the presence of an expanded Layer IV, which is further subdivided into sublayers to segregate thalamic input channels (Preuss, Qi, and Kaas 1999). By contrasting the primate data with the rest of the mammalian sample, we aimed to gain insights into the potential neural correlates of visual specialization within the primate lineage.

2 | Materials and Methods

2.1 | Sample Selection and Dissection

A total of 18 mammalian species were included in this study (Figure 1). Nonhuman tissue samples were obtained from various sources, including research centers and zoos. Each brain was collected postmortem. A small proportion of samples were fixed by means of vascular perfusion with 4% paraformaldehyde (PFA), whereas the majority were immersion fixed in 10% formalin (Table 1). The human brain sample was provided by the NIH NeuroBiobank from a young adult individual with no reported history of neurological or psychiatric disorders. The sample from a wild male African elephant (*L. africana*) came from an individual that was euthanized following population management decisions unrelated to any scientific study and prepared as described in Manger et al. (2009).

Brain mass was recorded at the time of extraction or upon receipt from the donating institutions. Postmortem intervals were recorded wherever possible and did not exceed 18 h for any of the individuals sampled. Ages at death of individuals in the sample were compared to the species-typical ages for sexual maturity and maximum life span (Tacutu et al. 2018); on this basis, all samples came from relatively young adult individuals, with the following exceptions: The giant anteater and two-toed sloth individuals were juvenile (less than the age of sexual maturity), and the clouded leopard, Kodiak bear, rock hyrax, and squirrel monkey individuals were elderly adults (ages in the upper quartile of the period from sexual maturity to maximum lifespan).

Following fixation, tissue blocks were dissected from the occipital pole. Comparative neuroanatomical studies have consistently identified the most posterior part of the occipital lobe as the location of Area V1 across mammalian species (Krubitzer 1995; Karlen and Krubitzer 2007). The dissected blocks were inclusive of the pial surface and the gray matter/white matter boundary to preserve orientation during processing. Tissue blocks were sectioned with a vibrating microtome to a thickness of 300 μm in a plane perpendicular to the pial surface.

10969861, 2024, 9, Downloaded from https://onlinelibrary.wiley.com/doi/10.1002/cne.25669 by University Of Witwatersrand, Wiley Online Library on [11/10/2024]. See the Terms and Conditions (https://onlinelibrary.wiley.com/terms-and-conditions) on Wiley Online Library for rules of use; OA articles are governed by the applicable Creative Commons License

TABLE 1 | Dataset used in this study.

Species	Common name	Age (years)	Sex	Hemisphere	Fixation	Brain mass (g)	Neuron density (mm^2)	Mitochondria density (mm^2)	Synapse density (mm^2)	PSD length (nm)
Bettongia penicillata	Bettong	10	Female	Right	Immersion	9.6	40,447	1214,281	632,260	388
Choloepus didactylus	Two-toed sloth	2	Female	Right	Immersion	36.0	17,425	1628,644	828,190	350
Dinomys branickii	Pacarana	11	Male	Right	Perfusion	36.3	13,537	1276,463	857,317	359
Giraffa camelopardalis	Giraffe	17	Female	Left	Immersion	675.0[a]	10,350	1123,306	662,832	344
Homo sapiens	Human	19	Male	Right	Immersion	1336.0[b]	7258	1318,314	672,542	352
Lemur catta	Ring-tailed lemur	16	Female	Right	Immersion	22.3	29,398	1560,863	571,193	317
Loxodonta africana	African bush elephant	Young adult	Male	Left	Perfusion	4835.0	3119	1455,067	732,506	310
Macropus rufogriseus	Bennett's wallaby	3	Male	Right	Immersion	28.2	23,211	1347,839	655,101	322
Mus musculus	Mouse	Adult	Male	Right	Perfusion	0.4	53,681	1287,821	870,361	262
Myrmecophaga tridactyla	Giant anteater	>1	Female	Right	Immersion	76.0	11,234	992,671	827,203	378
Neofelis nebulosa	Clouded leopard	14	Female	Left	Immersion	68.3[a]	13,736	1511,730	585,267	332
Pan troglodytes	Chimpanzee	23	Female	Left	Immersion	407.5	11,030	1459,302	800,016	339
Papio anubis	Olive baboon	7	Male	Right	Immersion	174.3	10,495	1678,743	578,396	299
Procavia capensis	Rock hyrax	1	Male	Right	Immersion	18.1	28,971	1071,012	709,600	331
Rangifer tarandus	Reindeer	7	Female	Left	Immersion	252.9	6635	1107,001	800,545	333
Saimiri sciureus	Squirrel monkey	25	Male	Right	Immersion	24.9	14,911	1245,053	571,222	307
Trichechus manatus	Manatee	Young adult	Female	Right	Perfusion	350.0	6258	1229,503	770,590	361
Ursus arctos	Kodiak bear	39	Female	Right	Immersion	385.0	9268	1100,947	598,439	403

Note: Fixation method indicates if samples were collected following vascular perfusion with 4% paraformaldehyde or if samples were immersion fixed in 10% formalin.

[a]Brain mass was recorded for only one hemisphere and doubled.

[b]No brain mass was recorded for this sample; therefore, the value used is the published average for male adults (Hartmann et al. 1994).

10969861, 2024, 9, Downloaded from https://onlinelibrary.wiley.com/doi/10.1002/cne.25669 by University Of Witwatersrand, Wiley Online Library on [11/10/2024]. See the Terms and Conditions (https://onlinelibrary.wiley.com/terms-and-conditions) on Wiley Online Library for rules of use; OA articles are governed by the applicable Creative Commons License

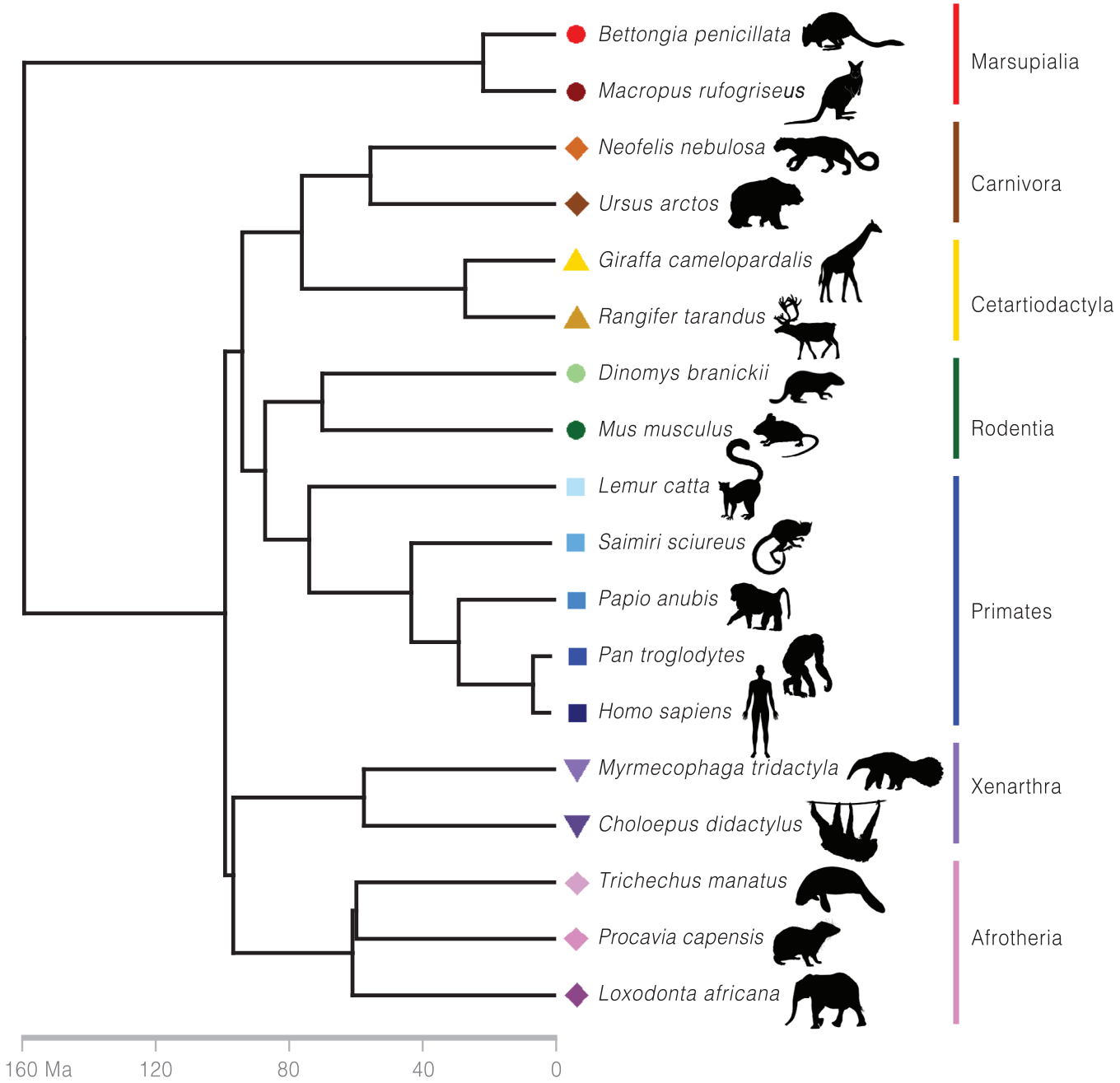


FIGURE 1 | Phylogenetic tree of the species included in this study, with the color and symbols of datapoints used to represent each species in Figures 4 and 6. The scale of the timeline at the bottom of the figure is in millions of years (Ma). *Source:* Phylogenetic tree obtained from timetree.org and animal silhouettes from phylopic.org.

2.2 | Sample Processing for Electron Microscopy

To investigate the ultrastructure of Area V1, electron microscopy was employed. Samples were rinsed with 0.1 M sodium cacodylate buffer and postfixed in 2% PFA and 2% glutaraldehyde in 0.1 M sodium cacodylate buffer for 24 h. Samples were further rinsed in cacodylate buffer and then fixed with 1% aqueous osmium tetroxide for 4–6 h. Following additional aqueous rinses, tissues were counter-stained en bloc with 1% aqueous uranyl acetate overnight, followed by graded ethanol and propylene oxide dehydration. Samples were then infiltrated with EmBed 812-based resin (Electron Microscopy Sciences, Catalog #14120) for 18–24 h and then polymerized at 60°C for a minimum of 48 h. Following curing, samples were trimmed and mounted for ultramicrotome sectioning. Ultrathin sections (80–120 nm) were obtained using a diamond knife on an ultramicrotome and collected on silicon wafers.

2.3 | Imaging

Images of Area V1 were captured using a Helios FIBSEM (focused ion beam scanning electron microscope, used without ion beam, FEI). Image tile scan acquisition and stitching were

10969861, 2024, 9, Downloaded from https://onlinelibrary.wiley.com/doi/10.1002/cne.25669 by University Of Witwatersrand, Wiley Online Library on [11/10/2024]. See the Terms and Conditions (https://onlinelibrary.wiley.com/terms-and-conditions) on Wiley Online Library for rules of use; OA articles are governed by the applicable Creative Commons License

performed using Thermo Scientific Maps software (version 3.11; RRID:SCR_024446), and pixel size was recorded independently for all images. We opted to employ two-dimensional (2D) imaging techniques rather than full three-dimensional (3D) ultrastructure reconstruction. This decision was driven by several key considerations to balance the need for broad comparative analysis with practical constraints. By focusing on 2D electron microscopy, we were able to include a larger number of species in our analysis. Although 3D reconstructions provide detailed visualization of cellular structures, due to the intense processing and computational requirements of the method, such studies generally are feasible only for a limited number of specimens within relatively restricted tissue volumes. By using 2D electron microscopy, we were able to efficiently process a larger number of individuals across phylogenetic diversity, enabling a broadly comparative analysis that would not have been possible with a 3D approach within the scope of this study.

One overview image per sample was acquired at 3500× magnification, with a dwell time of 3–5 μs. The overview images, which were used to count neurons, included the pial surface to the white matter boundary. These images were obtained at a resolution of 68.07 nm/pixel on average, depending on the overall field of view (*SEM* = 3.37 nm/pixel). Across the sample, the mean total size of overview images was 33,542.79 μm^2 (*SEM* = 3892.30 μm^2).

From the same samples, high-magnification images were acquired with a concentric back scatter (CBS) detector at an accelerating voltage of 4.5 kV and at a working distance of approximately 3.5–4 mm. Three images were acquired at 65,000× magnification from each specimen, with a dwell time of 3–5 μs. High-magnification images were acquired as long vertical tile scan strips through the depth of the cortex inclusive of the pial surface to the white matter boundary to provide sampling uniformity across the cortical layers (DeFelipe et al. 1999). These high-magnification tile scan images, which were used in the quantification of mitochondria and synapses, were obtained at a resolution of 4.1 nm/pixel. Resolution in the *z* axis (equivalent to section thickness) was 20 nm. Across the sample, high-magnification images were 4817.37 μm^2 in size on average (*SEM* = 557.01 μm^2).

2.4 | Quantification

Image quantification was performed using ImageJ software (version 1.53k, NIH; RRID:SCR_003070). Quantification employed an unbiased systematic sampling of counting frames (Colonnier and Beaulieu 1985; DeFelipe et al. 1999) selected from grid squares overlaid in a similar manner across all images of the same magnification (separate grid selection strategies were employed for overview vs. high-magnification image sets). The grid ensured uniform sampling and minimized selection bias. For all images, grids with an area of 500,000 square pixels were overlaid in an unbiased systematic manner, such that grid squares were not touching and were evenly spaced across the area of the image, from the pial surface to the white matter boundary (which was easily identified in overview images by the presence of abundant myelinated axons). Counting frames were selected as a fraction of the grid squares as described below.

Neurons were identified by their overall shape and size, as well as the presence of a nucleus containing a nucleolus (Peters, Palay, and Webster 1976). Neuronal nuclei were differentiated from nuclei of other cell types by one or more of the following criteria: the presence of a nucleolus, presence of a cellular "shadow" consistent with neuronal morphology, the overall size in comparison to the surrounding cells, and/or the lack of chromatin globules within the karyoplasm (Figure 2). Neurons were counted from every fourth grid square in overview images, yielding an average of 222.23 counting frames (*SEM* = 16.78). The counting frames had an average size of 34.03 μm^2 (*SEM* = 1.69 μm^2). Neurons falling within the counting frames were counted only when the center of the nucleus was located inside the frame to avoid double counting, especially at the frame boundaries. Only counting frames that were free of tissue processing artifacts were retained in the analysis. In all, this sampling approach investigated a mean of 22.55% of each image's surface area and a total of 98,030 μm^2 of tissue across individual specimens, resulting in 1584 neurons counted.

Due to the diverse nature of the sources of the brains in the sample and different necropsy procedures, variation in the quality of tissue preservation was evident, making it challenging to reliably classify synapses into symmetric and asymmetric types. Therefore, to ensure consistent and reliable measurements across all samples, we opted to examine total synapse density and PSD length, instead of subdividing synapses into specific types. Within these sample images, synapses were identified by one or more of the following features: an electron-dense synaptic cleft, presynaptic vesicles, presynaptic densities, and/or postsynaptic densities. All synapses were identified and counted regardless of the orientation of the synaptic cleft. We counted synapses present within the selected frames, ensuring that synaptic contacts crossing the frame boundaries were only counted if the presynaptic vesicles were visible within the frame. Mitochondria were identified on the basis of their characteristic morphology, including distinct double-membrane structures and folded cristae, giving them a darker and more dense appearance compared to large cellular vesicles or lysosomes.

Mitochondria and synapses were counted from three separate high-magnification tile scan images per sample (Figure 3) from every 12th grid square, yielding an average of 126.90 counting frames (*SEM* = 4.97) which were each 2.08 μm^2 in size. Only counting frames that were free of tissue processing artifacts were retained in the analysis. In total, this sampling approach investigated a mean of 5.47% of each image's surface area and a total of 14,157 μm^2 of tissue across specimens, resulting in counting 9459 synapses and 18,988 mitochondria.

For the measurement of PSD length, only those synapses where the synaptic cleft was clearly visible were included. This was to ensure the precision of the measurement, as an en face view or a cut that obscured the synaptic cleft could potentially lead to inaccurate length estimation. Measurement of PSD length was conducted using the line tool in ImageJ software. A mean of 105.36 PSDs were quantified per brain (minimum threshold per brain = 50, *SEM* = 7.64), which were selected in a systematic random fashion within sampling grid squares.

Measurements were conducted by at least two independent observers (MTK, KR, and CCS), with high levels of interobserver

10969861, 2024, 9, Downloaded from https://onlinelibrary.wiley.com/doi/10.1002/cne.25669 by University Of Witwatersrand, Wiley Online Library on [11/10/2024]. See the Terms and Conditions (https://onlinelibrary.wiley.com/terms-and-conditions) on Wiley Online Library for rules of use; OA articles are governed by the applicable Creative Commons License

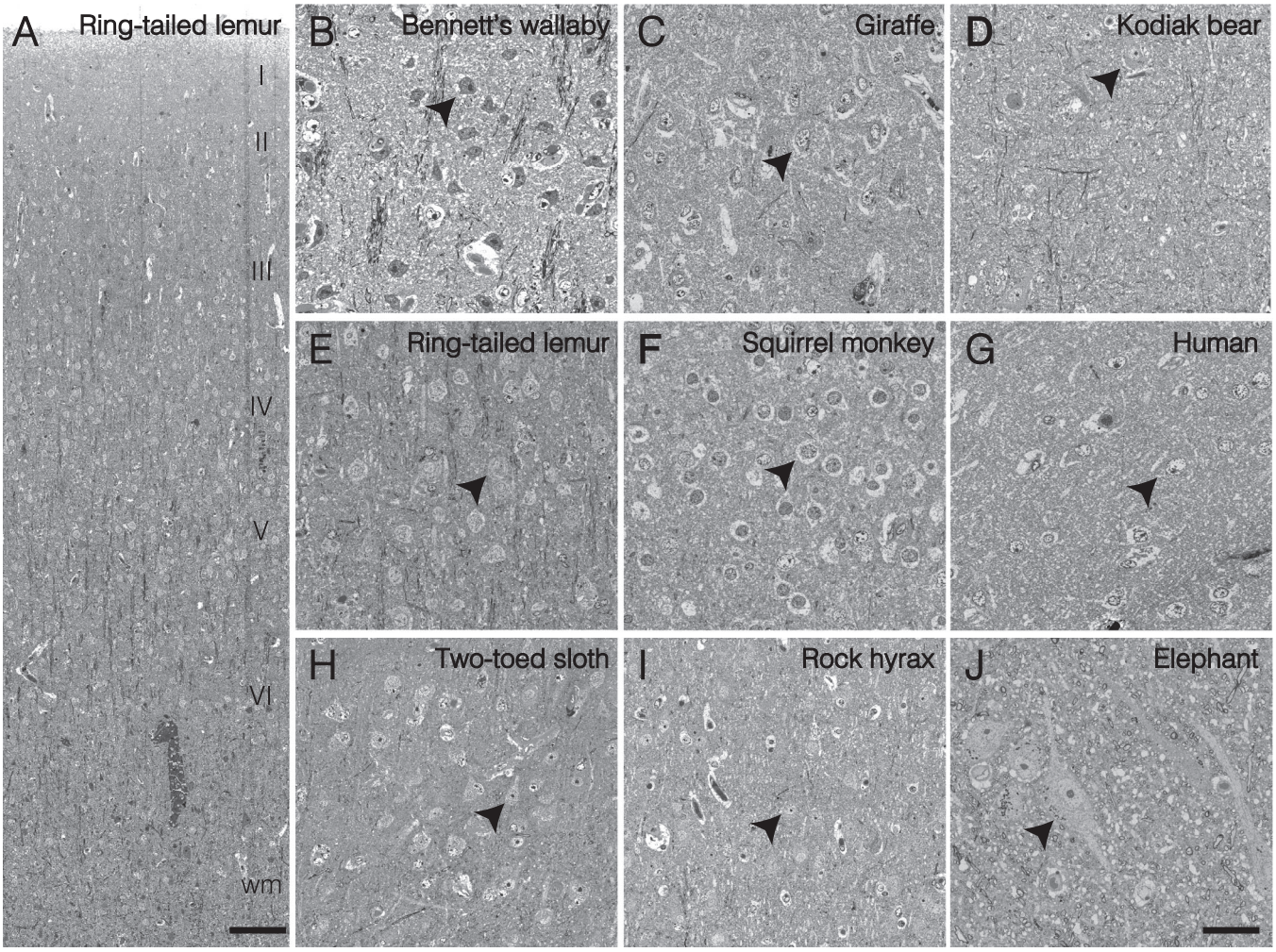


FIGURE 2 | Examples of images that were used for quantification of neuron densities. (A) The full cortical width of Area V1 in a ring-tailed lemur. Close-ups with arrowhead indicate one example neuron from each image in (B) Bennett's wallaby, (C) giraffe, (D) Kodiak bear, (E) ring-tailed lemur, (F) squirrel monkey, (G) human, (H) two-toed sloth, (I) rock hyrax, and (J) African elephant. Scale bar in (A) = 300 μm. Scale bar for all other images = 100 μm.

repeatability for neuron density ($r = 0.99$), mitochondria density ($r = 0.90$), and synapse density ($r = 0.83$).

The areal densities of neurons, synapses, and mitochondria were calculated as the total number of counted objects divided by the sum of the areas of the counting frames sampled. We did not apply size-frequency corrections to these density estimates, which are sometimes used to address the potential bias introduced by size differences in the structures being analyzed (Colonnier and Beaulieu 1985; DeFelipe et al. 1999; Peters, Moss, and Sethares 2001). These correction methods are applied when larger objects are more likely to intersect with the plane of histological sections, potentially leading to an overestimation of their frequency. In this study, counts of neuron density were based on the center of the nucleus, not total cellular size; therefore, without such correction, our counts of neuron density demonstrated scaling exponents against brain size that were congruent with previous studies (see Section 3). In addition, because our measurements showed that PSD length was remarkably uniform across species (see Section 3), the probability of intersection with the histological plane would be similar across species, despite the varying sizes of the brains, thereby minimizing the risk of overestimation of synapse density due to size differences. For mitochondria in 2D electron microscopy, size estimation is challenging due to anisotropy. Mitochondria can vary significantly in shape, often appearing as elongated or branched structures rather than perfect spheres.

2.5 | Data Analysis

Cellular and ultrastructural variables were averaged per sample, and the density per unit area was used for comparative analysis. The data frame was imported into R Studio (R Core Team), and subsequent calculations were made using R Project for Statistical Computing (RRID:SCR_001905). Brain mass for each sample was log transformed and compared against log transformed neuron density, mitochondria density, synapse density, and PSD length. A phylogeny of the species in this study was created using the TimeTree.org website (RRID:SCR_021162) (Kumar et al. 2017), and the newick file was transformed to nexus format using FigTree version 1.4.4 (RRID:SCR_008515). To analyze correlations and scaling, we used phylogenetic generalized least squares (pGLS) regression with a maximum likelihood estimation for

10969861, 2024, 9, Downloaded from https://onlinelibrary.wiley.com/doi/10.1002/cne.25669 by University Of Witwatersrand, Wiley Online Library on [11/10/2024]. See the Terms and Conditions (https://onlinelibrary.wiley.com/terms-and-conditions) on Wiley Online Library for rules of use; OA articles are governed by the applicable Creative Commons License

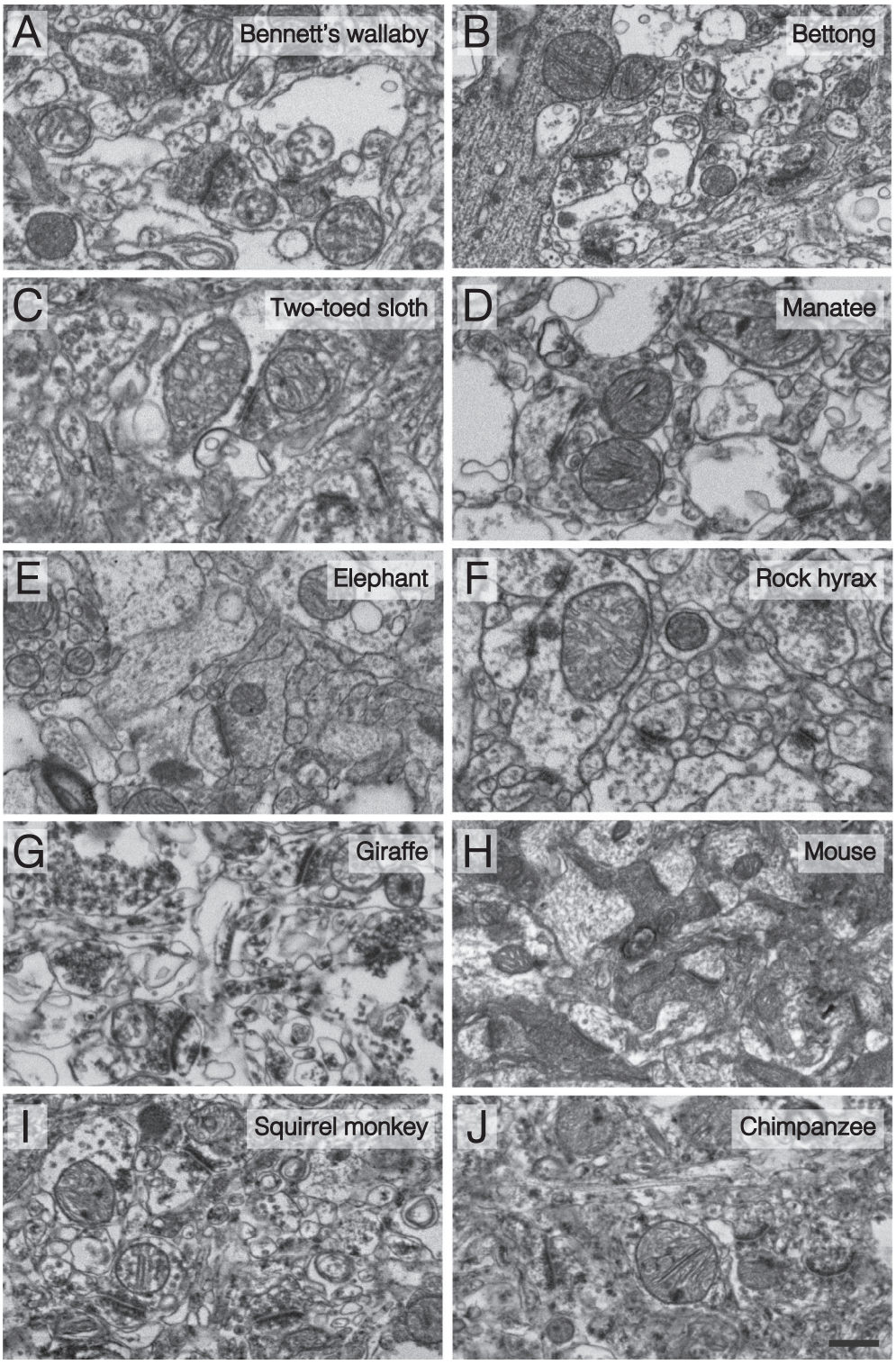


FIGURE 3 | Examples of images that were used for quantification of synapses and mitochondria: (A) Bennett's wallaby, (B) bettong, (C) two-toed sloth, (D) manatee, (E) African elephant, (F) rock hyrax, (G) giraffe, (H) mouse, (I) squirrel monkey, and (J) chimpanzee. Scale bar = 600 nm.

the value of the phylogenetic signal parameter (lambda, λ). All measures were regressed against brain mass to examine scaling relationships and against each other to investigate the associations of their interspecific variation (Hollenbeck 2005; Ly and Verstreken 2006; Picard 2015; Yu et al. 2020). Although pGLS was applied to all analyses to account for nonindependence in the distribution of values among the species in the sample, it should be noted that Pagel's lambda (λ), a measure of phylogenetic signal, was found to be zero in all regressions. This means that the values of the species in the dataset are not influenced by their phylogenetic relationships and pGLS regressions are equivalent to ordinary least squares regressions. Comparisons between primate and non-primate species were also conducted to explore differences in synaptic and mitochondria variables.

10969861, 2024, 9, Downloaded from https://onlinelibrary.wiley.com/doi/10.1002/cne.25669 by University Of Witwatersrand, Wiley Online Library on [11/10/2024]. See the Terms and Conditions (https://onlinelibrary.wiley.com/terms-and-conditions) on Wiley Online Library for rules of use; OA articles are governed by the applicable Creative Commons License

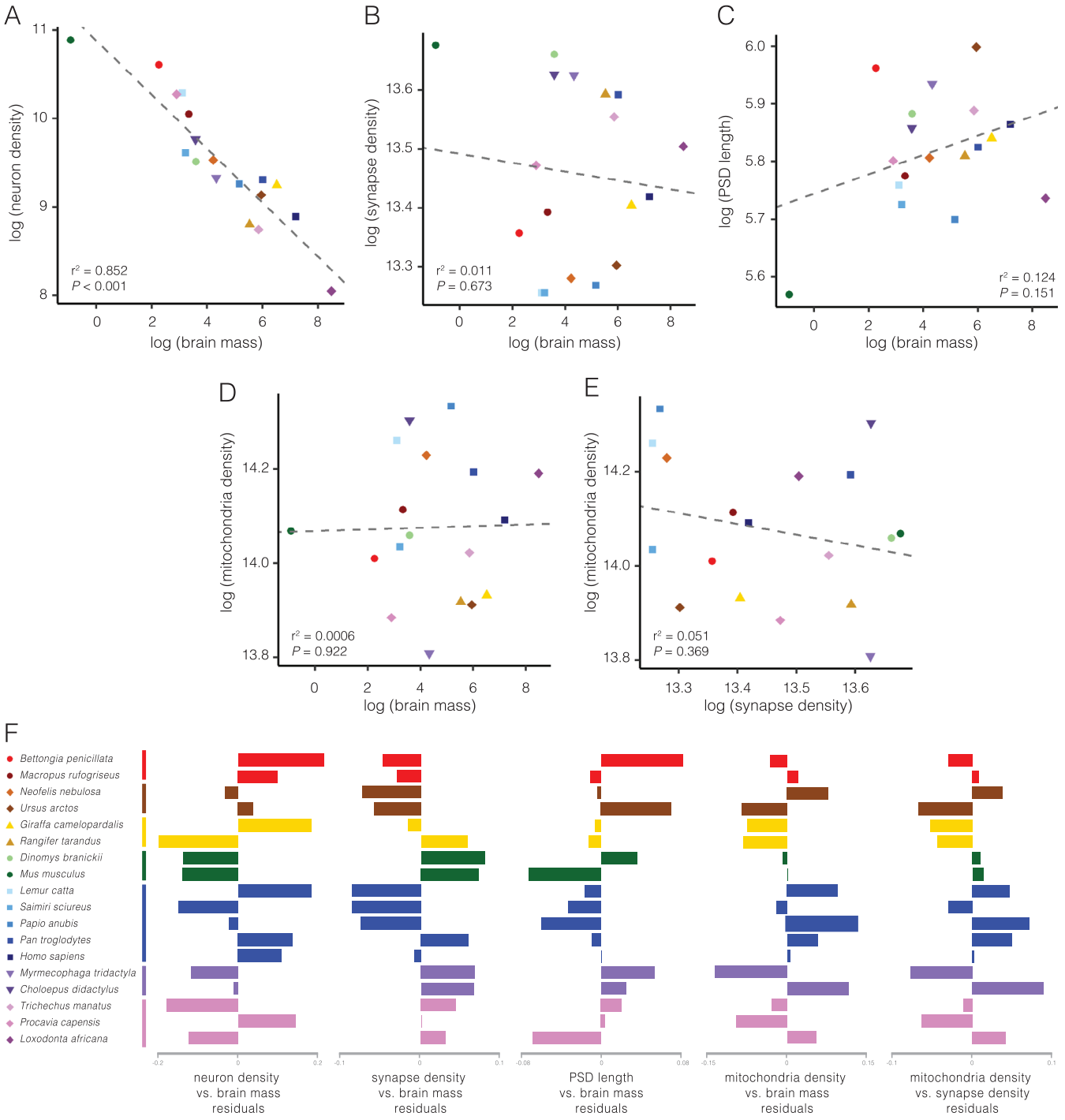


FIGURE 4 | pGLS regressions (gray dashed line in all plots) of log transformed (A) neuron density as a function of brain mass, (B) synapse density as a function of brain mass, (C) PSD length as a function of brain mass, (D) mitochondria density as a function of brain mass, (E) mitochondria density as a function of synapse density, and (F) residuals from these regressions. PSD, postsynaptic density.

3 | Results

As observed in previous comparative datasets (Haug 1987; Lewitus, Sherwood, and Hof 2012; Sherwood et al. 2007; Tower 1954), neuron density in this sample displayed a significant negative relationship with brain mass ($r^2 = 0.852$, $b = -0.306$, $F_{1,16} = 91.9$, $p = 4.933e-08$) (Figure 4).

The regression of synapse density against brain mass was not significant ($r^2 = 0.011$, $b = -0.008$, $F_{1,16} = 0.185$, $p = 0.673$), and the 95% confidence intervals of the scaling coefficient included zero (−0.045, 0.030) (Figure 4). This indicates that synapse density in Area V1 is relatively invariant across this sample of brains. The overall average synapse density across species was 706,865 synapses/mm^2 ($SD = 106,263$; range = 1.5-fold).

10969861, 2024, 9, Downloaded from https://onlinelibrary.wiley.com/doi/10.1002/cne.25669 by University Of Witwatersrand, Wiley Online Library on [11/10/2024]. See the Terms and Conditions (https://onlinelibrary.wiley.com/terms-and-conditions) on Wiley Online Library for rules of use; OA articles are governed by the applicable Creative Commons License

PSD length in Area V1 was also not significantly associated with brain size ($r^2 = 0.124$, $b = 0.017$, $F_{1,16} = 2.27$, $p = 0.151$), and the 95% confidence intervals of the scaling coefficient were nearly zero (0.004, 0.030) (Figure 4). The overall average PSD length across species was 338 nm ($SD = 33.91$; range = 1.5-fold).

In addition, the regression of mitochondria density against brain mass was not significant ($r^2 = 0.0006$, $b = 0.002$, $F_{1,16} = 0.010$, $p = 0.922$), and the 95% confidence intervals of the scaling coefficient included zero (−0.034, 0.038) (Figure 4). The overall average mitochondria density across species was 1311,587 mitochondria/mm^2 ($SD = 200{,}731$; range = 1.7-fold).

We tested whether mitochondria density was associated with synapse density and found that they were independent of each other ($r^2 = 0.051$, $b = -0.228$, $F_{1,16} = 0.857$, $p = 0.369$).

Next, we examined each ultrastructural variable between primates ($n = 5$) and non-primates ($n = 13$) using Welch's two-sample t-tests with unequal variance. We found no significant differences between groups for synapse density ($t_{7.31} = -1.80$, $p = 0.114$), PSD length ($t_{12.23} = -1.50$, $p = 0.158$), or mitochondria density ($t_{7.77} = 2.07$, $p = 0.074$), and a difference approaching significance for mitochondria per synapse to be greater in primates than other mammals ($t_{5.91} = 2.43$, $p = 0.052$) (Figure 5).

Finally, we calculated the number of synapses per neuron (S/N) and mitochondria per neuron (M/N) across the full sample of mammals. Results showed that both S/N and M/N increase as a function of brain mass enlargement (S/N: $r^2 = 0.756$, $b = 0.299$, intercept = 2.609, $F_{1,16} = 49.4$, $p = 2.847\text{e} - 06$; M/N: $r^2 = 0.829$, $b = 0.308$, intercept = 3.186, $F_{1,16} = 77.6$, $p = 1.554\text{e} - 07$) (Figure 6). Analysis of covariance to compare the two regressions indicated that scaling slopes for S/N and M/N did not differ from each other ($F = 0.028$, $p = 0.867$); however, the intercept for M/N was higher than for S/N ($F = 121.455$, $p = 1.996\text{e} - 12$). This shows that S/N and M/N scale with a common allometric relationship, with an overall average of 1.9 mitochondria for every synapse in Area V1 across mammals.

4 | Discussion

Our investigation into the ultrastructural characteristics of the primary visual cortex (Area V1) across mammalian species sheds light on the scaling relationships of synapses, PSD length, mitochondria, and neurons in the context of brain size and phylogenetic diversity. The results of this study show that synapse and mitochondria density, as well as PSD length, are relatively invariant across mammals with widely varying brain sizes and cortical neuron densities, suggesting that these features are evolutionarily conserved due to the crucial roles they play in neural function and metabolic consumption within the cerebral cortex.

4.1 | Invariants in Cortical Design

Across the sample of mammal brains, we found that cortical synapse density, PSD length, and mitochondria density values were within only a 1.5–1.7-fold range of variation. Previous studies have similarly shown that cortical synapse density varies minimally among cortical regions in humans, rhesus macaques, and mice (Cano-Astorga et al. 2023; Gilman, Medalla, and Luebke 2017; Rakic et al. 1986), and independently of brain size among primates (Sherwood et al. 2020) and among diverse mammals in a sample of eight species compiled from data in the literature (Karbowski 2014). However, one study found that the somatosensory cortex of Etruscan shrews, which have the smallest brains among living mammals, exhibits synaptic densities nearly three times higher than those observed in the human temporal and entorhinal cortex (Alonso-Nanclares et al. 2023). The study highlights the substantial contribution of an especially thick cortical Layer I in Etruscan shrews due to its high synaptic density on apical dendritic tufts.

Our results point to factors that limit PSD length within a narrow range of variation among mammals. Proteins within the PSD are involved in signaling cascades that regulate synaptic function, including receptor trafficking, synaptic vesicle recycling, and cytoskeletal reorganization (Wang and Konopka 2012). The length of the PSD is correlated with the number of synaptic receptors and scaffolding proteins, which can impact the postsynaptic neuron's responsiveness to neurotransmitter release from the presynaptic neuron (Sheng and Hoogenraad 2007). The PSD length also contributes to the organization and positioning of neurotransmitter receptors at the synapse, which can influence the efficiency of signal transmission and the integration of synaptic inputs. Changes in synaptic activity can lead to alterations in PSD length, and these modifications are associated with synaptic plasticity, such as long-term potentiation (LTP) and long-term depression (LTD). Even as synaptic sizes may exhibit plasticity, the average length of excitatory synapses does not undergo significant change during postnatal development or aging (Huttenlocher and Dabholkar 1997; Peters, Sethares, and Luebke 2008; Zecevic and Rakic 1991). Furthermore, comparative studies of human and mouse PSD proteomes find a high degree of compositional conservation for key proteins (Bayés et al. 2012). Our results indicate that there is an optimal PSD length with a mean of 338 nm that is necessary to house the complement of proteins required for adequate synaptic function in mammals. This is congruent with other comparative studies that have similarly found relative uniformity of synaptic lengths across various cortical areas in smaller samples of mammals (Alonso-Nanclares et al. 2023; DeFelipe, Alonso-Nanclares, and Arellano 2002; Karbowski 2014).

It has been noted that other characteristics of the cerebral cortex are also independent of brain size (Karbowski 2014). Previous research has shown that the ratio of excitatory to inhibitory synapses is conserved across mammals, with excitatory synapses comprising about 80%–90% of the total in the cerebral cortex (Alonso-Nanclares et al. 2023; DeFelipe, Alonso-Nanclares, and Arellano 2002). In addition, diameters of intracortical axons and dendrites also do not systematically change with brain size (Braitenberg and Schüz 1998; Karbowski 2014). The existence of such evolutionarily conserved invariants suggests universal cortical design principles, prompting questions about their causes and interrelations.

10969861, 2024, 9, Downloaded from https://onlinelibrary.wiley.com/doi/10.1002/cne.25669 by University Of Witwatersrand, Wiley Online Library on [11/10/2024]. See the Terms and Conditions (https://onlinelibrary.wiley.com/terms-and-conditions) on Wiley Online Library for rules of use; OA articles are governed by the applicable Creative Commons License

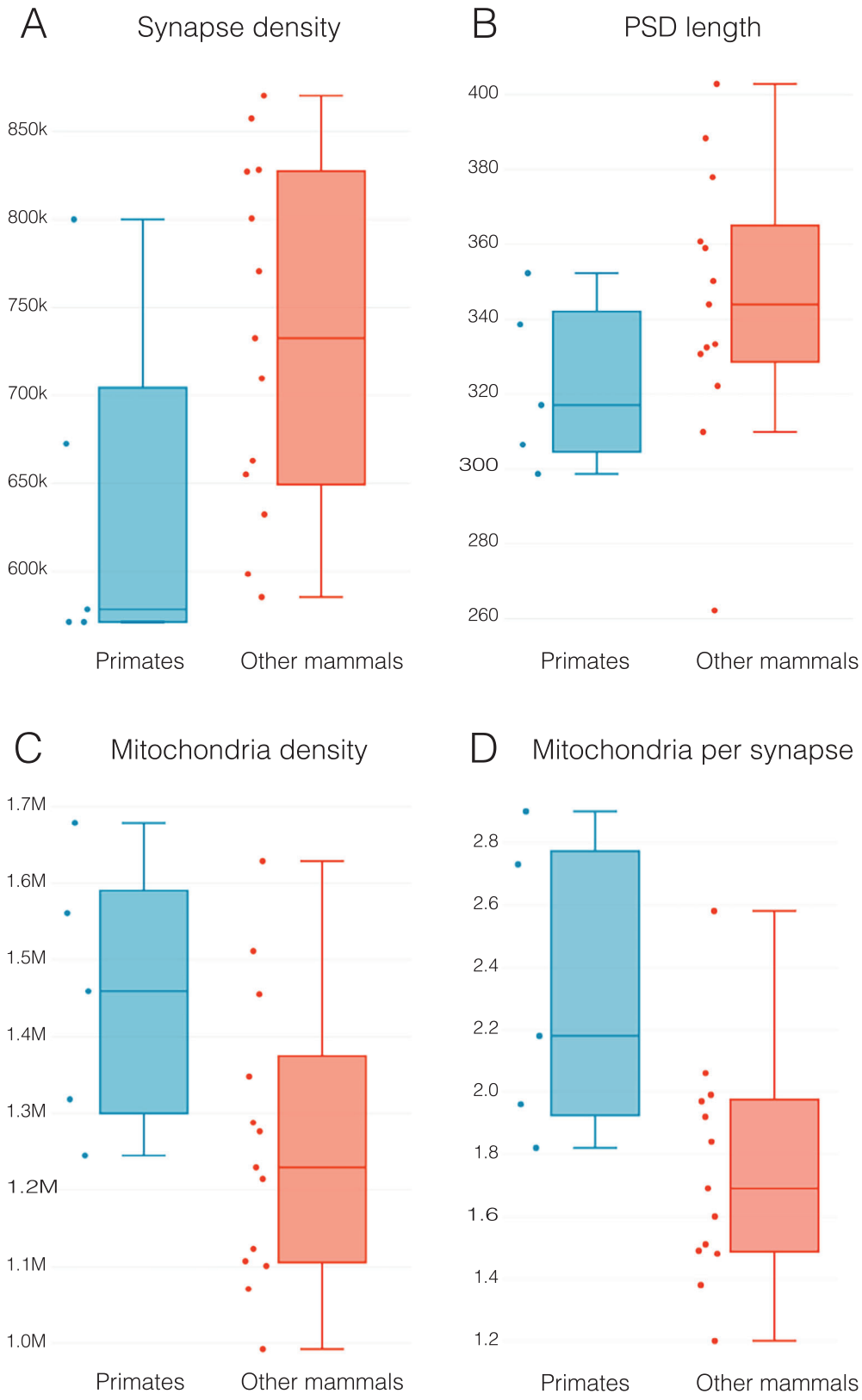


FIGURE 5 | Box and whisker plots comparing ultrastructure variables between primates and other mammals showing median and interquartiles: (A) synapse density (mm^2), (B) PSD length (nm), (C) mitochondria density (mm^2), and (D) mitochondria per synapse. None of the variables differed significantly between primates and other mammals. PSD, postsynaptic density.

10969861, 2024, 9, Downloaded from https://onlinelibrary.wiley.com/doi/10.1002/cne.25669 by University Of Witwatersrand, Wiley Online Library on [11/10/2024]. See the Terms and Conditions (https://onlinelibrary.wiley.com/terms-and-conditions) on Wiley Online Library for rules of use; OA articles are governed by the applicable Creative Commons License

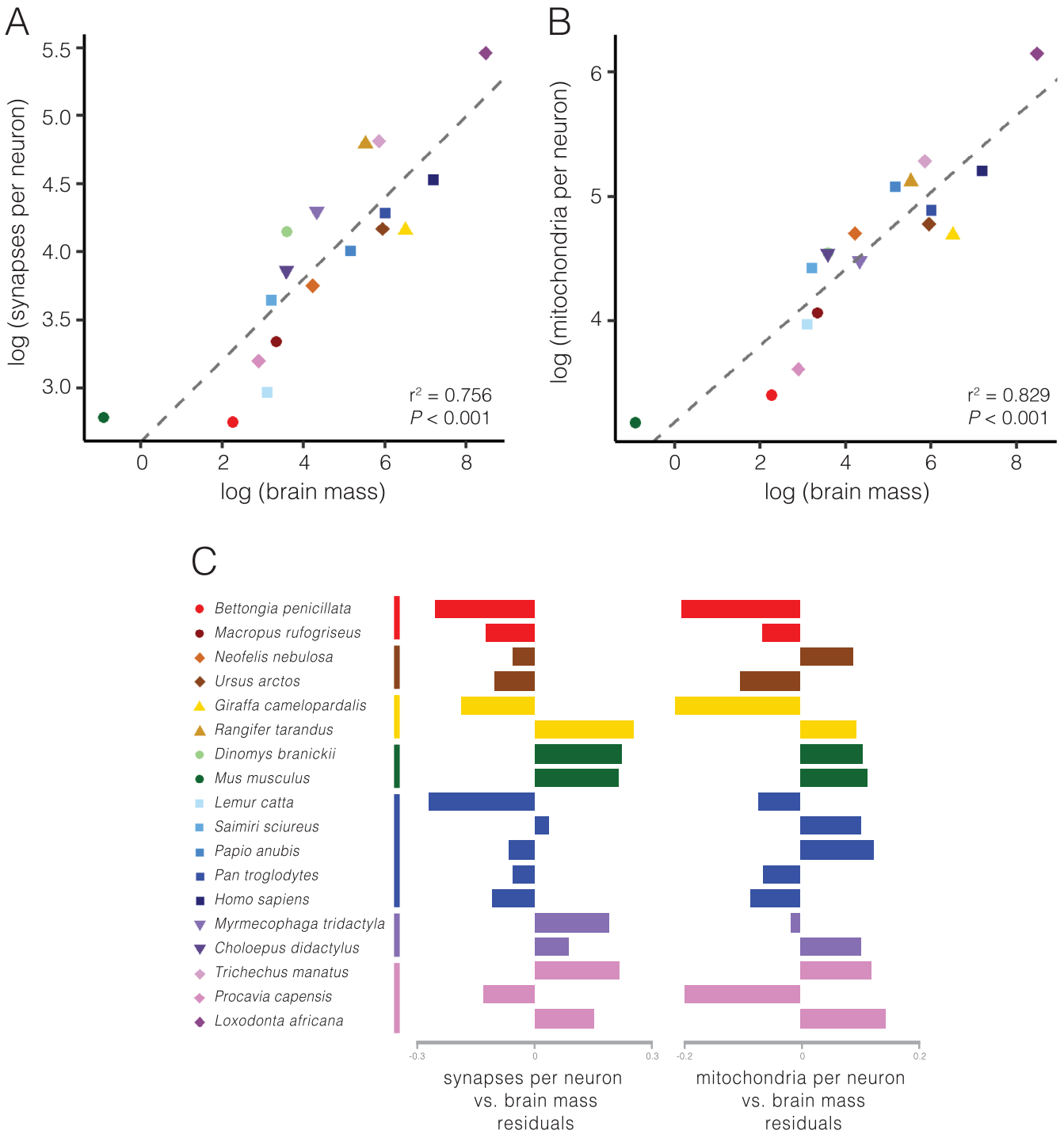


FIGURE 6 | pGLS regression (gray dashed line in all plots) of log transformed (A) synapses per neuron as a function of brain mass, (B) mitochondria per neuron as a function of brain mass, and (C) residuals from these regressions.

4.2 | Mitochondria and Synaptic Metabolism

Maintaining a relatively constant synapse and mitochondria density could be an adaptive strategy to optimize energy usage. Cerebral metabolic rate per volume decreases with increasing brain size at an exponent of approximately −0.15 (Castrillon et al. 2023; Karbowski 2014). This indicates that as brains enlarge, they become more energetically efficient per unit volume due to metabolic scaling, in a manner similar to the body as a whole (Kleiber 1947; Schmidt-Nielsen 1984). The maintenance of a relatively constant synaptic density across species, as observed in the cerebral cortex in the current study, could contribute to this efficiency by ensuring that the metabolic demands of sustaining neural activity are met without causing an unsustainable increase in energy consumption.

The observed average of 1.9 mitochondria per synapse across the diverse spectrum of mammalian species signifies a fundamental

10969861, 2024, 9, Downloaded from https://onlinelibrary.wiley.com/doi/10.1002/cne.25669 by University Of Witwatersrand, Wiley Online Library on [11/10/2024]. See the Terms and Conditions (https://onlinelibrary.wiley.com/terms-and-conditions) on Wiley Online Library for rules of use; OA articles are governed by the applicable Creative Commons License

interdependence between mitochondrial distribution and synaptic function. It is notable that the number of mitochondria per synapse was somewhat higher in primates than other mammals, possibly reflecting specializations for visual function, although the small sample size warrants caution in this interpretation. The positioning of mitochondria in close proximity to synaptic clefts is due to their pivotal role in shaping the bioenergetic landscape of synapses, acting as dynamic hubs for energy production, buffering of calcium, and the regulation of redox signaling (Harris, Jolivet, and Attwell 2012). Additional non-synaptic mitochondria are located mostly within dendrites (Santuy, Turégano-López et al. 2018). The relatively consistent proportion of mitochondria to synapses across widely different brain sizes indicates potential mechanisms to safeguard the reliability of synaptic activity. The metabolic and ionic buffering role of mitochondria may act to prevent faulty neurotransmission and excitotoxicity (Datta and Jaiswal 2021). Mitochondria can rapidly respond to fluctuations in energy requirements during synaptic transmission (Hollenbeck 2005; Lennie 2003; Ly and Verstreken 2006). This ensures a resilient and consistent energy supply, allowing synapses to sustain their signaling processes even in the face of varying energetic challenges.

In addition to mitochondria, research has also shown that synapses are dependent on other microstructural elements that are involved in the delivery of energy, such as cerebral vasculature and glia. The energy available in the cortex is constrained in part by the geometric design of the microvascular system, with neuro-hemodynamic coupling that is bidirectional between neurons and blood flow (Moore and Cao 2008). Capillaries comprise about 1%–2% of cortical volume across adult mammals, regardless of brain size (Karbowski 2014). Counts of densities of neurons and non-neuronal cells (mostly glia) in a sample of more than 60 mammalian species found that non-neuronal cells varied by only ~10-fold, whereas neuron densities varied by ~1000-fold (Herculano-Houzel and Dos Santos 2018), suggesting a relatively constant density of glia due to their volume-related essential functions, including providing structural support, maintaining homeostasis, insulating axons, participating in synaptic communication, and contributing to immune responses. Although systematic counts of the various types of astrocytes, oligodendrocytes, and microglia have not yet been conducted across a large comparative mammalian sample, it is notable that one study of protoplasmic interlaminar astrocytes in 46 species found that they differed minimally in density within the cerebral cortex (Falcone et al. 2019). Interlaminar astrocytes may participate in a wide variety of functions, including neurotransmitter reuptake and release, pyruvate metabolism, reactive oxygen species removal, antioxidant metabolism, blood brain barrier regulation, ion buffering, and the synthesis and secretion of trophic factors. In addition, a study of microglia in 33 species found that they also had a relatively invariant density across brain regions and species (Dos Santos et al. 2020). Microglia play a multifaceted role in synaptic function, including involvement in synaptic pruning, immune response, modulation of synaptic plasticity, and maintenance of homeostasis. Understanding these interrelationships among mitochondria, synapses, glia, and microvasculature provides a perspective on the regularities across mammals in the metabolic maintenance of cortical neural circuits (Hyder, Rothman, and Bennett 2013).

4.3 | Primate-Specific Features and Visual Specialization

Despite the well-documented visual adaptations and associated neural specializations in primates (Heesy and Ross 2001; Rosa and Tweedale 2005), the ultrastructural characteristics of primate Area V1 that we examined in the current study did not generally differ from other mammalian species. The absence of distinctive ultrastructural features in primates underscores the importance of other adaptations that contribute to their exceptional visual abilities at the level of retinal specializations, connectivity patterns, and cortical processing hierarchies (Kaas 2012; Leopold, Mitchell, and Freiwald 2017). Thus, these circuit-level adaptations in the primate visual cortex occur in the context of conservation of overall synapse and mitochondria distributions in Area V1. Understanding this interplay between derived and conserved features will provide a more comprehensive perspective on the evolutionary mechanisms that have shaped the distinct visual capabilities of primates.

4.4 | Scaling Relationships and Brain Enlargement

In the current study and previous research (Haug 1987; Lewitus, Sherwood, and Hof 2012; Sherwood et al. 2007; Tower 1954), it has been demonstrated that neuron density decreases in association with brain enlargement across mammals. Because of the uniformity of synapse and mitochondria density, we found that larger brained mammals, such as elephants and humans, exhibit proportionally more synapses and mitochondria per neuron compared to smaller brained mammals, like mice. The common allometric relationship between synapses and mitochondria per neuron suggests a coordinated scaling mechanism that likely reflects the balance between energy turnover and information signaling.

These results expand on previous studies that have shown that larger brains are characterized by cortical pyramidal neurons with greater dendritic branching and an increased total number of synaptic spines (Elston et al. 2006; Galakhova et al. 2022; Jacobs et al. 2018). The extended dendritic arbors allow for a higher degree of connectivity, enabling the integration of a larger number of synaptic inputs and enhanced computational capacity. Cerebral metabolic utilization, which is limited by the factors described above, is distributed among cortical neurons. Thus, as cortical neurons become increasingly complex, only a subset can be active at any given time to encode units of information (Olshausen and Field 2004). This sparse coding strategy is thought to enhance information processing by reducing redundancy in neural activity and preserving energy. Furthermore, the biophysical properties of larger cortical neurons in mammalian species with bigger brains have been shown to exhibit lower average firing rates (Karbowski 2009) and higher membrane ionic conductance, which cancels out the decrease in surface-to-volume ratio, to maintain a constant conductance per unit cerebral volume across species (Beaulieu-Laroche et al. 2021). Thus, optimization of energy utilization could be a key factor in shaping the computational demands of larger brains with more complex neurons connected in extended networks.

10969861, 2024, 9, Downloaded from https://onlinelibrary.wiley.com/doi/10.1002/cne.25669 by University Of Witwatersrand, Wiley Online Library on [11/10/2024]. See the Terms and Conditions (https://onlinelibrary.wiley.com/terms-and-conditions) on Wiley Online Library for rules of use; OA articles are governed by the applicable Creative Commons License

4.5 | Future Directions

A key limitation of our study involves the reliance on 2D quantification. Although 2D electron microscopy sections provide valuable insights, 3D volumetric measurements can offer a more accurate representation of synapse and mitochondria dimensions. Another limitation of our study is the potential specificity of our findings to the primary visual cortex. It is important to consider that the patterns we observe may not be generalizable to other cortical regions. For instance, Hsu, Luebke, and Medalla (2017) reported no significant difference in PSD 3D area between mice and rhesus monkeys in Area V1 but found larger PSD areas in the frontal cortex of mice compared to monkeys. Similarly, Benavides-Piccione et al. (2002) observed larger spines in human pyramidal cells compared to those in mice in the temporal and occipital cortex. Furthermore, in our study, mitochondria were counted across the entire sampled volume without distinguishing their specific locations. The ratio of 1.9 mitochondria per synapse thus represents an average density across the whole Area V1 cortical volume, rather than being specific to synaptic boutons. This lack of specificity may obscure the functional implications of mitochondrial density for synaptic energy expenditure, as the energy demands and efficacy of synapses are closely linked to the presence of mitochondria in boutons and axons, as highlighted in previous studies (Smith et al. 2016; Lees, Johnson, and Ashby 2020).

Future investigations should conduct more in-depth analysis of asymmetric and symmetric synapse types in a greater number of cortical areas, among layers, and within a broader sample of species. 3D mapping could also be used to allow for a better understanding of the relationship between cortical neuron types and the cell-intrinsic features analyzed in this study. Specifically, variables that could be the focus of additional studies include the shape of synapses (macular, perforated, and horseshoe-shaped) and the postsynaptic targets of asymmetric and symmetric synapses (axospinous and axodendritic). For instance, as axodendritic synapses are, on average, larger than the more prevalent axospinous synapses (Santuy, Rodríguez et al. 2018), contrasting these two types of synapses can provide insight as to whether synaptic size affects function. Research on synaptic shapes is also currently scarce, though previous research in the hippocampus has found that initiating LTP can alter the relative amounts of the different synaptic shapes (Santuy, Rodríguez et al. 2018). As a result, further investigation of synapse shapes could reveal possible similarities and differences in their roles across species. In addition, future comparative studies should focus on quantifying mitochondria more specifically within synaptic boutons and axons, as this would provide a more precise understanding of their role in supporting synaptic function. This distinction is crucial for interpreting the functional significance of mitochondrial distribution in relation to synaptic energy dynamics.

Our study provides insights into the ultrastructural scaling of the primary visual cortex across diverse mammalian species. The invariance in synapse density, PSD length, and mitochondria density suggests that there are energetic constraints that are scale-free as brains vary in size. Overall, these findings shed light on the functional importance of synaptic and mitochondrial characteristics and their relationship to brain size in mammals. Although this study analyzed a small number of individuals from each species and a single cortical region of interest, it represents the first of its kind to analyze ultrastructure across such a wide range of species. The results are relevant to our understanding of phylogenetic variation in cellular energy consumption, synaptic information processing, and neural transmission in the cerebral cortex.

Author Contributions

M.T.K. and C.C.S. conceptualized the study. C.C.S. and P.R.M. obtained and prepared the brains used in this study. M.T.K. and Y.D.K. performed the electron microscopy. M.T.K., K.R., and C.C.S. performed the analysis. M.T.K. and C.C.S. wrote the initial draft of the manuscript, with all authors contributing to the editing and improvement of the early drafts of the manuscript. All authors had full access to all data in the study and took responsibility for the integrity of the data and the accuracy of the data analysis.

Acknowledgments

We thank Elaine Miller, Dr. Andrew Barr, and Dr. Robert H. Miller for their useful feedback on the development of this project. We thank the GW Nanofabrication and Imaging Center for expert technical assistance. We acknowledge Cleveland Metroparks Zoo, Smithsonian National Zoological Park, Milwaukee County Zoo, and the National Chimpanzee Brain Resource (funded by NIH NS092988) for contributing brain specimens used in this study.

Ethics Statement

All experimental procedures with postmortem tissue were carried out according to the National Institutes of Health guidelines for animal research and were approved by the Institutional Animal Care and Use Committee (IACUC) and Institutional Review Board (IRB) at The George Washington University.

Conflicts of Interest

The authors declare no conflicts of interest.

Data Availability Statement

All quantitative data are available in Table 1.

Peer Review

The peer review history for this article is available at https://publons.com/publon/10.1002/cne.25669.

References

Alonso-Nanclares, L., J. Gonzalez-Soriano, J. R. Rodriguez, and J. DeFelipe. 2008. "Gender Differences in Human Cortical Synaptic Density." *Proceedings of the National Academy of Sciences of the United States of America* 105, no. 38: 14615–14619.

Alonso-Nanclares, L., J. R. Rodríguez, A. Merchan-Perez, et al. 2023. "Cortical Synapses of the World's Smallest Mammal: An FIB/SEM Study in the Etruscan Shrew." *Journal of Comparative Neurology* 531, no. 3: 390–414.

Assaf, Y., A. Bouznach, O. Zomet, A. Marom, and Y. Yovel. 2020. "Conservation of Brain Connectivity and Wiring Across the Mammalian Class." *Nature Neuroscience* 23, no. 7: 805–808.

Attwell, D., and S. B. Laughlin. 2001. "An Energy Budget for Signaling in the Grey Matter of the Brain." *Journal of Cerebral Blood Flow & Metabolism* 21, no. 10: 1133–1145.

10969861, 2024, 9, Downloaded from https://onlinelibrary.wiley.com/doi/10.1002/cne.25669 by University Of Witwatersrand, Wiley Online Library on [11/10/2024]. See the Terms and Conditions (https://onlinelibrary.wiley.com/terms-and-conditions) on Wiley Online Library for rules of use; OA articles are governed by the applicable Creative Commons License

Barton, R. A., and P. H. Harvey. 2000. "Mosaic Evolution of Brain Structure in Mammals." *Nature* 405, no. 6790: 1055–1058.

Bayés, A., M. O. Collins, M. D. Croning, L. N. van de Lagemaat, J. S. Choudhary, and S. G. Grant. 2012. "Comparative Study of Human and Mouse Postsynaptic Proteomes Finds High Compositional Conservation and Abundance Differences for Key Synaptic Proteins." *PLoS One* 7, no. 10: e46683.

Beaulieu-Laroche, L., N. J. Brown, M. Hansen, et al. 2021. "Allometric Rules for Mammalian Cortical Layer 5 Neuron Biophysics." *Nature* 600, no. 7888: 274–278.

Benavides-Piccione, R., I. Ballesteros-Yáñez, J. DeFelipe, and R. Yuste. 2002. "Cortical Area and Species Differences in Dendritic Spine Morphology." *Journal of Neurocytology* 31, no. 3–5: 337–346.

Boddy, A. M., M. R. McGowen, C. C. Sherwood, L. I. Grossman, M. Goodman, and D. E. Wildman. 2012. "Comparative Analysis of Encephalization in Mammals Reveals Relaxed Constraints on Anthropoid Primate and Cetacean Brain Scaling." *Journal of Evolutionary Biology* 25, no. 5: 981–994.

Braitenberg, V., and A. Schüz. 1998. *Cortex: Statistics and Geometry of Neuronal Connectivity*. Berlin: Springer.

Cano-Astorga, N., S. Plaza-Alonso, J. DeFelipe, and L. Alonso-Nanclares. 2023. "3D Synaptic Organization of Layer III of the Human Anterior Cingulate and Temporopolar Cortex." *Cerebral Cortex* 33, no. 17: 9691–9708.

Castrillon, G, S. Epp, A. Bose, et al. 2023. "An Energy-Costly Architecture of Neuromodulators for Human Brain Evolution and Cognition." *Science Advances* 9, no. 50: eadi7632.

Chan, D. C. 2006. "Mitochondrial Fusion and Fission in Mammals." *Annual Review of Cell and Developmental Biology* 22, no. 1: 79–99.

Colonnier, M., and C. Beaulieu. 1985. "An Empirical Assessment of Stereological Formulae Applied to the Counting of Synaptic Disks in the Cerebral Cortex." *Journal of Comparative Neurology* 231, no. 2: 175–179.

Datta, S., and M. Jaiswal. 2021. "Mitochondrial Calcium at the Synapse." *Mitochondrion* 59: 135–153.

DeCasien, A. R., and J. P. Higham. 2019. "Primate Mosaic Brain Evolution Reflects Selection on Sensory and Cognitive Specialization." *Nature Ecology & Evolution* 3, no. 10: 1483–1493.

DeFelipe, J., L. Alonso-Nanclares, and J. I. Arellano. 2002. "Microstructure of the Neocortex: Comparative Aspects." *Journal of Neurocytology* 31, no. 3–5: 299–316.

DeFelipe, J., P. Marco, I. Busturia, and A. Merchán-Pérez. 1999. "Estimation of the Number of Synapses in the Cerebral Cortex: Methodological Considerations." *Cerebral Cortex (New York, N.Y.: 1991)* 9, no. 7: 722–732.

Dos Santos, S. E., M. Medeiros, J. Porfirio, et al. 2020. "Similar Microglial Cell Densities Across Brain Structures and Mammalian Species: Implications for Brain Tissue Function." *Journal of Neuroscience* 40, no. 24: 4622–4643.

Douglas, R. J., and K. A. C. Martin. 2004. "Neuronal Circuits of the Neocortex." *Annual Review of Neuroscience* 27, no. 1: 419–451.

Else, P., and A. Hulbert. 1985. "An Allometric Comparison of the Mitochondria of Mammalian and Reptilian Tissues: The Implications for the Evolution of Endothermy." *Journal of Comparative Physiology. B, Biochemical, Systemic, and Environmental Physiology* 156: 3–11.

Elston, G. N., R. Benavides-Piccione, A. Elston, et al. 2006. "Specializations of the Granular Prefrontal Cortex of Primates: Implications for Cognitive Processing." *Anatomical Record Part A: Discoveries in Molecular, Cellular, and Evolutionary Biology* 288, no. 1: 26–35.

Elston, G. N., R. Benavides-Piccione, A. Elston, P. R. Manger, and J. DeFelipe. 2011. "Pyramidal Cells in Prefrontal Cortex of Primates: Marked Differences in Neuronal Structure Among Species." *Frontiers in Neuroanatomy* 5: 2.

Englund, M., and L. Krubitzer. 2022. "Phenotypic Alterations in Cortical Organization and Connectivity Across Different Time Scales." *Brain, Behavior and Evolution* 97, no. 1–2: 108–120.

Falcone, C., M. Wolf-Ochoa, S. Amina, et al. 2019. "Cortical Interlaminar Astrocytes Across the Therian Mammal Radiation." *Journal of Comparative Neurology* 527, no. 10: 1654–1674.

Fox, K. C. R., M. Muthukrishna, and S. Shultz. 2017. "The Social and Cultural Roots of Whale and Dolphin Brains." *Nature Ecology & Evolution* 1, no. 11: 1699–1705.

Friedman, J. R., and J. Nunnari. 2014. "Mitochondrial Form and Function." *Nature* 505, no. 7483: 335–343.

Galakhova, A. A., S. Hunt, R. Wilbers, et al. 2022. "Evolution of Cortical Neurons Supporting Human Cognition." *Trends in Cognitive Sciences* 26, no. 11: 909–922.

García-Cabezas, M. Á., and B. Zikopoulos. 2019. "Evolution, Development, and Organization of the Cortical Connectome." *PLoS Biology* 17, no. 5: e3000259.

Gilman, J. P., M. Medalla, and J. I. Luebke. 2017. "Area-Specific Features of Pyramidal Neurons—A Comparative Study in Mouse and Rhesus Monkey." *Cerebral Cortex* 27, no. 3: 2078–2094.

Hara, Y., F. Yuk, R. Puri, W. G. M. Janssen, P. R. Rapp, and J. H. Morrison. 2014. "Presynaptic Mitochondrial Morphology in Monkey Prefrontal Cortex Correlates With Working Memory and Is Improved With Estrogen Treatment." *Proceedings of the National Academy of Sciences of the United States of America* 111, no. 1: 486–491.

Harris, J. J., R. Jolivet, and D. Attwell. 2012. "Synaptic Energy Use and Supply." *Neuron* 75, no. 5: 762–777.

Hartmann, P., A. Ramseier, F. Gudat, M. J. Mihatsch, and W. Polasek. 1994. "Normal Weight of the Brain in Adults in Relation to Age, Sex, Body Height, and Weight." *Pathologe* 15, no. 3: 165–170. https://doi.org/10.1007/s002920050040.

Haug, H. 1987. "Brain Sizes, Surfaces, and Neuronal Sizes of the Cortex Cerebri: A Stereological Investigation of Man and His Variability and a Comparison With Some Mammals (Primates, Whales, Marsupials, Insectivores, and One Elephant)." *American Journal of Anatomy* 180, no. 2: 126–142.

Heesy, C. P., and C. F. Ross. 2001. "Evolution of Activity Patterns and Chromatic Vision in Primates: Morphometrics, Genetics and Cladistics." *Journal of Human Evolution* 40, no. 2: 111–149.

Heldstab, S. A., Z. K. Kosonen, S. E. Koski, J. M. Burkart, C. P. van Schaik, and K. Isler. 2016. "Manipulation Complexity in Primates Coevolved With Brain Size and Terrestriality." *Scientific Reports* 6: 24528.

Herculano-Houzel, S. 2009. "The Human Brain in Numbers: A Linearly Scaled-Up Primate Brain." *Frontiers in Human Neuroscience* 3: 31.

Herculano-Houzel, S. 2011. "Scaling of Brain Metabolism With a Fixed Energy Budget per Neuron: Implications for Neuronal Activity, Plasticity and Evolution." *PLoS One* 6, no. 3: e17514.

Herculano-Houzel, S., and S. E. Dos Santos. 2018. "You Do Not Mess With the Glia." *Neuroglia* 1: 193–219.

Herculano-Houzel, S., P. R. Manger, and J. H. Kaas. 2014. "Brain Scaling in Mammalian Evolution as a Consequence of Concerted and Mosaic Changes in Numbers of Neurons and Average Neuronal Cell Size." *Frontiers in Neuroanatomy* 8: 77.

Hollenbeck, P. J. 2005. "Mitochondria and Neurotransmission: Evacuating the Synapse." *Neuron* 47: 331–333.

Hsu, A., J. I. Luebke, and M. Medalla. 2017. "Comparative Ultrastructural Features of Excitatory Synapses in the Visual and Frontal Cortices of the Adult Mouse and Monkey." *Journal of Comparative Neurology* 525, no. 9: 2175–2191.

Huttenlocher, P. R., and A. S. Dabholkar. 1997. "Regional Differences in Synaptogenesis in Human Cerebral Cortex." *Journal of Comparative Neurology* 387: 167–178.

10969861, 2024, 9, Downloaded from https://onlinelibrary.wiley.com/doi/10.1002/cne.25669 by University Of Witwatersrand, Wiley Online Library on [11/10/2024]. See the Terms and Conditions (https://onlinelibrary.wiley.com/terms-and-conditions) on Wiley Online Library for rules of use; OA articles are governed by the applicable Creative Commons License

Hyder, F., D. L. Rothman, and M. R. Bennett. 2013. "Cortical Energy Demands of Signaling and Non-Signaling Components in the Brain Are Conserved Across Mammalian Species and Activity Levels." *Proceedings of the National Academy of Sciences of the United States of America* 110, no. 9: 3549–3554.

Jacobs, B., M. E. Garcia, N. B. Shea-Shumsky, et al. 2018. "Comparative Morphology of Gigantopyramidal Neurons in Primary Motor Cortex Across Mammals." *Journal of Comparative Neurology* 526, no. 3: 496–536.

Kaas, J. H. 2012. "The Evolution of Neocortex in Primates." *Progress in Brain Research* 195: 91–102.

Kaas, J. H. 2013. "The Evolution of Brains From Early Mammals to Humans." *Wiley Interdisciplinary Reviews: Cognitive Science* 4, no. 1: 33–45.

Karbowski, J. 2009. "Thermodynamic Constraints on Neural Dimensions, Firing Rates, Brain Temperature, and Size." *Journal of Computational Neuroscience* 27, no. 4: 415–436.

Karbowski, J. 2014. "Constancy and Trade-Offs in the Neuroanatomical and Metabolic Design of the Cerebral Cortex." *Frontiers in Neural Circuits* 8: 9.

Karlen, S. J., and L. Krubitzer. 2007. "The Functional and Anatomical Organization of Marsupial Neocortex: Evidence for Parallel Evolution Across Mammals." *Progress in Neurobiology* 82, no. 3: 122–141.

Kleiber, M. 1947. "Body Size and Metabolic Rate." *Physiological Reviews* 27: 511–541.

Krubitzer, L. 1995. "The Organization of Neocortex in Mammals: Are Species Differences Really So Different?." *Trends in Neurosciences* 18, no. 9: 408–417.

Kukat, C., C. A. Wurm, H. Spahr, M. Falkenberg, N.-G. Larsson, and S. Jakobs. 2011. "Super-Resolution Microscopy Reveals That Mammalian Mitochondrial Nucleoids Have a Uniform Size and Frequently Contain a Single Copy of mtDNA." *Proceedings of the National Academy of Sciences of the United States of America* 108, no. 33: 13534–13539.

Kumar, S., G. Stecher, M. Suleski, and S. B. Hedges. 2017. "TimeTree: A Resource for Timelines, Timetrees, and Divergence Times." *Molecular Biology and Evolution* 34, no. 7: 1812–1819.

La Rosa, C., F. Cavallo, A. Pecora, et al. 2020. "Phylogenetic Variation in Cortical Layer II Immature Neuron Reservoir of Mammals." *Elife* 9: e55456.

Lees, R. M., J. D. Johnson, and M. C. Ashby. 2020. "Presynaptic Boutons That Contain Mitochondria Are More Stable." *Frontiers in Synaptic Neuroscience* 11: 37.

Lennie, P. 2003. "The Cost of Cortical Computation." *Current Biology* 13, no. 6: 493–497.

Leopold, D. A., J. F. Mitchell, and W. A. Freiwald. 2017. "Evolved Mechanisms of High-Level Visual Perception in Primates." In *Evolution of Nervous Systems*, edited by J. Kaas, 203–235. Amsterdam, the Netherlands: Elsevier.

Lewitus, E., C. C. Sherwood, and P. R. Hof. 2012. "Cellular Signatures in the Primary Visual Cortex of Phylogeny and Placentation." *Brain Structure and Function* 217, no. 2: 531–547.

Liu, Y. T., C. L. Tao, P. M. Lau, Z. H. Zhou, and G. Q. Bi. 2019. "Postsynaptic Protein Organization Revealed by Electron Microscopy." *Current Opinion in Structural Biology* 54: 152–160.

Ly, C. V., and P. Verstreken. 2006. "Mitochondria at the Synapse." *Neuroscientist* 12, no. 4: 291–299.

MacLean, E. L., B. Hare, C. L. Nunn, et al. 2014. "The Evolution of Self-Control." *Proceedings of the National Academy of Sciences of the United States of America* 111, no. 20: E2140–E2148.

Magistretti, P. J., and I. Allaman. 2015. "A Cellular Perspective on Brain Energy Metabolism and Functional Imaging." *Neuron* 86, no. 4: 883–901.

Manger, P. R., P. Pillay, B. C. Maseko, et al. 2009. "Acquisition of Brains From the African Elephant (*Loxodonta africana*): Perfusion-Fixation and Dissection." *Journal of Neuroscience Methods* 179, no. 1: 16–21.

Moore, C. I., and R. Cao. 2008. "The Hemo-Neural Hypothesis: On the Role of Blood Flow in Information Processing." *Journal of Neurophysiology* 99, no. 4: 2035–2047.

Morozov, Y. M., D. Datta, C. D. Paspalas, and A. F. T. Arnsten. 2017. "Ultrastructural Evidence for Impaired Mitochondrial Fission in the Aged Rhesus Monkey Dorsolateral Prefrontal Cortex." *Neurobiology of Aging* 51: 9–18.

Nguyen, V. T., R. Uchida, A. Warling, et al. 2020. "Comparative Neocortical Neuromorphology in Felids: African Lion, African Leopard, and Cheetah." *Journal of Comparative Neurology* 528, no. 8: 1392–1422.

Olshausen, B. A., and D. J. Field. 2004. "Sparse Coding of Sensory Inputs." *Current Opinion in Neurobiology* 14, no. 4: 481–487.

Peters, A., M. B. Moss, and C. Sethares. 2001. "The Effects of Aging on Layer 1 of Primary Visual Cortex in the Rhesus Monkey." *Cerebral Cortex* 11, no. 2: 93–103.

Peters, A., S. L. Palay, and H. deF. Webster. 1976. *The Fine Structure of the Nervous System: Neurons and Their Supporting Cells*. Oxford, UK: Oxford University Press.

Peters, A., C. Sethares, and J. I. Luebke. 2008. "Synapses Are Lost During Aging in the Primate Prefrontal Cortex." *Neuroscience* 152: 970–981.

Picard, M. 2015. "Mitochondrial Synapses: Intracellular Communication and Signal Integration." *Trends in Neurosciences* 38, no. 8: 468–474.

Preuss, T. M., H. Qi, and J. H. Kaas. 1999. "Distinctive Compartmental Organization of Human Primary Visual Cortex." *Proceedings of the National Academy of Sciences of the United States of America* 96, no. 20: 11601–11606.

Rakic, P., J. P. Bourgeois, M. F. Eckenhoff, N. Zecevic, and P. S. Goldman-Rakic. 1986. "Concurrent Overproduction of Synapses in Diverse Regions of the Primate Cerebral Cortex." *Science* 232, no. 4747: 232–235.

Rosa, M. G., and R. Tweedale. 2005. "Brain Maps, Great and Small: Lessons From Comparative Studies of Primate Visual Cortical Organization." *Philosophical Transactions of the Royal Society B: Biological Sciences* 360, no. 1456: 665–691.

Santuy, A., J. R. Rodríguez, J. DeFelipe, and A. Merchán-Pérez. 2018. "Study of the Size and Shape of Synapses in the Juvenile Rat Somatosensory Cortex With 3D Electron Microscopy." *Eneuro* 5, no. 1: ENEURO.0377–17.2017.

Santuy, A., M. Turégano-López, J. R. Rodríguez, L. Alonso-Nanclares, J. DeFelipe, and A. Merchán-Pérez. 2018. "A Quantitative Study on the Distribution of Mitochondria in the Neuropil of the Juvenile Rat Somatosensory Cortex." *Cerebral Cortex* 28, no. 10: 3673–3684.

Schmidt-Nielsen, K. 1984. *Scaling: Why Is Animal Size So Important?*. Cambridge: Cambridge University Press.

Sheng, M., and C. C. Hoogenraad. 2007. "The Postsynaptic Architecture of Excitatory Synapses: A More Quantitative View." *Annual Review of Biochemistry* 76: 823–847.

Sherwood, C. C., S. B. Miller, M. Karl, et al. 2020. "Invariant Synapse Density and Neuronal Connectivity Scaling in Primate Neocortical Evolution." *Cerebral Cortex* 30, no. 10: 5604–5615.

Sherwood, C. C., M. A. Raghanti, C. D. Stimpson, et al. 2007. "Scaling of Inhibitory Interneurons in Areas V1 and V2 of Anthropoid Primates as Revealed by Calcium-Binding Protein Immunohistochemistry." *Brain, Behavior and Evolution* 69, no. 3: 176–195.

Sherwood, C. C., C. D. Stimpson, C. Butti, et al. 2009. "Neocortical Neuron Types in Xenarthra and Afrotheria: Implications for Brain Evolution in Mammals." *Brain Structure and Function* 213, no. 3: 301–328.

Smaers, J. B., R. S. Rothman, D. R. Hudson, et al. 2021. "The Evolution of Mammalian Brain Size." *Science Advances* 7, no. 18: eabe2101.

Smith, H. L., J. N. Bourne, G. Cao, et al. 2016. "Mitochondrial Support of Persistent Presynaptic Vesicle Mobilization With Age-Dependent Synaptic Growth After LTP." *Elife* 5: e15275.

10969861, 2024, 9, Downloaded from https://onlinelibrary.wiley.com/doi/10.1002/cne.25669 by University Of Witwatersrand, Wiley Online Library on [11/10/2024]. See the Terms and Conditions (https://onlinelibrary.wiley.com/terms-and-conditions) on Wiley Online Library for rules of use; OA articles are governed by the applicable Creative Commons License

Sokoloff, L. 1981. "Localization of Functional Activity in the Central Nervous System by Measurement of Glucose Utilization With Radioactive Deoxyglucose." *Journal of Cerebral Blood Flow & Metabolism* 1, no. 1: 7–36.

Stimpson, C. D., J. B. Smaers, M. A. Raghanti, et al. 2023. "Evolutionary Scaling and Cognitive Correlates of Primate Frontal Cortex Microstructure." *Brain Structure and Function* Advance Online Publication. https://doi.org/10.1007/s00429-023-02719-7.

Tacutu, R., D. Thornton, E. Johnson, et al. 2018. "Human Ageing Genomic Resources: New and Updated Databases." *Nucleic Acids Research* 46, no. D1: D1083–D1090.

Tower, D. B. 1954. "Structural and Functional Organization of Mammalian Cerebral Cortex; the Correlation of Neurone Density With Brain Size; Cortical Neurone Density in the Fin Whale (*Balaenoptera physalus* L.) With a Note on the Cortical Neurone Density in the Indian Elephant." *Journal of Comparative Neurology* 101, no. 1: 19–51.

Vannucci, S. J., R. R. Clark, E. Koehler-Stec, et al. 1998. "Glucose Transporter Expression in Brain: Relationship to Cerebral Glucose Utilization." *Developmental Neuroscience* 20, no. 4–5: 369–379.

Ventura-Antunes, L., O. M. Dasgupta, and S. Herculano-Houzel. 2022. "Resting Rates of Blood Flow and Glucose Use per Neuron Are Proportional to Number of Endothelial Cells Available per Neuron Across Sites in the Rat Brain." *Frontiers in Integrative Neuroscience* 16: 821850.

Wang, G. Z., and G. Konopka. 2012. "Differential Functional Constraints on the Evolution of Postsynaptic Density Proteins in Neocortical Laminae." *PLoS One* 7, no. 6: e39686.

Yu, R., U. Lendahl, M. Nistér, and J. Zhao. 2020. "Regulation of Mammalian Mitochondrial Dynamics: Opportunities and Challenges." *Frontiers in Endocrinology* 11: 374.

Zecevic, N., and P. Rakic. 1991. "Synaptogenesis in Monkey Somatosensory Cortex." *Cerebral Cortex* 1: 510–523.

10969861, 2024, 9, Downloaded from https://onlinelibrary.wiley.com/doi/10.1002/cne.25669 by University Of Witwatersrand, Wiley Online Library on [11/10/2024]. See the Terms and Conditions (https://onlinelibrary.wiley.com/terms-and-conditions) on Wiley Online Library for rules of use; OA articles are governed by the applicable Creative Commons License